Published in final edited form as:

*ACS Chem Neurosci*. 2018 May 16; 9(5): 1066–1073. doi:10.1021/acschemneuro.7b00458.

# In Vivo Characterization of Two $^{18}$F-Labeled PDE10A PET Radioligands in Nonhuman Primate Brains

**Hui Liu**[†], **Hongjun Jin**[†], **Zonghua Luo**[†], **Xuyi Yue**[†], **Xiang Zhang**[†], **Hubert Flores**[‡], **Yi Su**[†], **Joel S. Perlmutter**[†,‡,§], and **Zhude Tu**[*,†]

[†]Department of Radiology, Physical Therapy and Occupational Therapy, Washington University School of Medicine, St. Louis, Missouri 63110, United States

[‡]Department of Neurology, Physical Therapy and Occupational Therapy, Washington University School of Medicine, St. Louis, Missouri 63110, United States

[§]Department of Neuroscience, Physical Therapy and Occupational Therapy, Washington University School of Medicine, St. Louis, Missouri 63110, United States

## Abstract

Positron emission tomography with phosphodiesterase 10A (PDE10A) specific radioligands provides a noninvasive and quantitative imaging tool to access the expression of this enzyme in vivo under normal and diseased conditions. We recently reported two potent $^{18}$F-labeled PDE10A radioligands ($^{18}$F-TZ19106B and $^{18}$F-TZ8110); initial evaluation in rats and nonhuman primates indicated stable metabolic profiles and excellent target-to-nontarget ratio (striatum/cerebellum) for both tracers. Herein, we focused on in vivo characterization of $^{18}$F-TZ19106B and $^{18}$F-TZ8110 to identify a suitable radioligand for imaging PDE10A in vivo. We directly compared microPET studies of these two radiotracers in adult male *Macaca fascicularis* nonhuman primates (NHPs). $^{18}$F-TZ19106B had higher striatal uptake and tracer retention in NHP brains than $^{18}$F-TZ8110, quantified by either standardized uptake values (SUVs) or nondisplaceable binding potential ($BP_{ND}$) estimated using reference-based modeling analysis. Blocking and displacement studies using the PDE10A inhibitor MP-10 indicated the binding of $^{18}$F-TZ19106B to PDE10A was specific and reversible. We also demonstrated sensitivity of $^{18}$F-TZ19106B binding to varying number of specific binding sites using escalating doses of MP-10 blockade (0.3, 0.5, 1.0, 1.5, and 2.0 mg/kg). Pretreatment with a dopamine D2-like receptor antagonist enhanced the striatal uptake of $^{18}$F-TZ19106B. Our results indicate that $^{18}$F-TZ19106B is a promising radioligand candidate for imaging PDE10A in vivo and it may be used to determine target engagement of PDE10A inhibitors and serve as a tool to evaluate the effect of novel antipsychotic therapies.

[*]**Corresponding Author**: Tel.: 314-362-8487. Fax: 314-362-8555. tuz@mir.wustl.edu.

**ORCID**

Zhude Tu: 0000-0003-0325-835X

**Author Contributions**

H.L., H.J., and Z.T. conceived the project and designed the experiments. H.L., H.J., Z.L., X.Y., X.Z., and H.F. performed the experiments and data analysis. H.L., H.J., J.S.P., and Z.T. wrote the manuscript. All authors edited and approved the final version of the manuscript.

**Notes**

The authors declare no competing financial interest.

## Graphical abstract

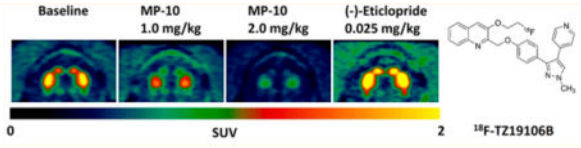


### Keywords

Phosphodiesterase 10A; PET radioligands; brain imaging; in vivo characterization; nonhuman primates; psychotic disorders

## INTRODUCTION

Phosphodiesterase 10A (PDE10A) is a dual-substrate specific phosphodiesterase that mostly occurs on striatal medium spiny neurons (MSNs)[1] including direct (mostly dopaminergic (DA) D1-like receptor mediated) and indirect pathway neurons (mostly DA D2-like receptor mediated).[2–4] PDE10A is primarily membrane-bound and associated with postsynaptic densities on dendritic spines.[3,5] Under normal conditions, the activation of D1-like receptor in MSNs upregulates cyclic adenosine monophosphate (cAMP) production, whereas D2-like receptor activation reduces cAMP production.[2,6] Accordingly, excessive striatal DA release exerts differential effects on the regulation of PDE10A in the two striatal output pathways. PDE10A would shift toward a somatic, cytosolic localization in D1-like mediated MSNs caused by increased PDE10A, whereas it may shift to an axonal and dendritic localization in D2-like MSNs caused by disinhibition of PDE10A palmitoylation.[7] Whether dopaminergic signaling modulates PDE10A function remains obscure but DA depletion alters PDE10A expression at both RNA and protein levels.[8] PDE10A mRNA levels were decreased in ipsilateral striatal neurons 10 weeks after unilateral 6-hydroxydopamine lesion in a rat model of nigrostriatal injury. PDE10A protein levels and activity also decreased in striatal neurons and in striatopallidal and striatonigral projections. Thus, PDE10A levels respond to nigrostriatal injury and may provide a postsynaptic biomarker for striatal function.

The interaction between PDE10A and DA receptors was also investigated by applying PDE10A inhibitors. PDE10A inhibitors suppress D2-like receptors and concomitantly potentiate D1-like receptor-mediated neurotransmission, which reflect desirable antipsychotic effects.[9] In direct pathway neurons, PDE10A inhibition by papaverine activates cAMP/protein kinase A (PKA) signaling, leading to potentiation of D1-like receptor signaling. In indirect pathway neurons, PDE10A inhibition by papaverine also activates cAMP/PKA signaling by simultaneously potentiating adenosine A2A receptor signaling and inhibiting D2-like receptor signaling. The balance of cAMP/PKA signaling between the direct and indirect pathways determines the output from basal ganglia.[10] PDE10A inhibitors activate cAMP/PKA signaling in indirect and direct pathway neurons, but predominately affect indirect pathway neurons. Experimental support of this comes from an electrophysiology study showing PDE10A inhibition has a greater facilitatory effect on corticostriatal synaptic activity in indirect pathway neurons.[11] Biochemical action of PDE10A inhibitors resembles antipsychotic drugs that act primarily as D2-like receptor

antagonists and increase dopamine- and cAMP-regulated neuronal phosphoprotein (DARPP-32) phosphorylation in indirect pathway neurons.[12] Thus, PDE10A radioligands have the potential to provide a metric of target engagement for novel antipsychotic therapies.

The first PDE10A PET radiotracer, carbon-11 labeled papaverine was radiolabeled and evaluated in 2010.[13] Due to the low retention of $^{11}$C-papaverine in the brain, tremendous efforts have been paid to develop a more suitable radioligand for imaging PDE10A in vivo. Currently, there are several lead PDE10A radioligands (Figure 1); all of them showed potent binding affinity and good selectivity toward PDE10A. Several of these radiotracers already have been transferred into clinical settings, including 18F-JNJ42259152,[14,15] 11C-IMA107,[16–19] $^{11}$C-Lu AE92686,[20,21] $^{18}$F-MNI-659,[22–25] and 11C-T-773.[26] MP-10 is the first generation of PDE10A compounds for treating schizophrenia, and was successfully radiolabeled with C-11 for in vivo evaluation. However, nonpolar radio-metabolites hampered its further application.[27,28] TZ1964B was developed and optimized based on MP-10[29] by changing its in vivo pathway of metabolism. We radiolabeled TZ1964B on the opposite side to avoid nonpolar radiometabolites that could cross the blood brain barrier,[30] and in vitro and in vivo characterization of 11C-TZ1964B in rodents and NHPs[31] demonstrated that $^{11}$C-TZ1964B is a suitable radioligand for imaging PDE10A.

Encouraged by the promising result of $^{11}$C-TZ1964B studies, our group recently explored and synthesized a series of PDE10A compounds for F-18 labeling, since F-18 labeled radioligands have several advantages over C-11 radiotracers in general, including longer half-life, better image resolution, and potential for delivery to off-site imaging facilities within a 3–4 h drive distance. Two new potent compounds were identified and radiolabeled: $^{18}$F-TZ19106B (named as $^{18}$F-20a), 3-(2-[$^{18}$F]-fluoroethoxy)-2-((4-(1-methyl-4-(pyridin-4-yl)-1*H*-pyrazol-3-yl)phenoxy)methyl) quinolone, and 18F-TZ8110 (named as $^{18}$F-18d), 4-(2-[$^{18}$F]Fluoroethoxy)-2-((4-(1-methyl-4-(pyridin-4-yl)-1H-pyrazol-3-yl)phenoxy)methyl) quinolone.[32] Initial evaluation in rats and nonhuman primates indicated that both radiotracers have good stability in vivo and excellent target-to-nontarget ratio (striatum/cerebellum),[32] although $^{18}$F-TZ19106B is even more stable than $^{18}$F-TZ8110. Therefore, the goal of the current study was to further investigate the in vivo binding properties of 18F-TZ19106B and 18F-TZ8110 through kinetic modeling, and identify a suitable radioligand for imaging PDE10A in vivo.

## RESULTS AND DISCUSSION

### MicroPET Baseline Scans in Nonhuman Primates

We previously reported high tracer accumulation in striatum and rapid clearance from nontarget brain regions of $^{18}$F-TZ19106B and $^{18}$F-TZ8110 in nonhuman primates.[32] To quantitatively compare the imaging properties of the two PDE10A tracers, 3 h dynamic PET studies were performed in male adult macacca fascicularis. Tissue time activity curves showed that both tracers had high uptake in NHP striatum, while $^{18}$F-TZ19106B had much higher striatal retention than $^{18}$F-TZ8110. Tracer uptake of $^{18}$F-TZ19106B in NHP striatum reached the max SUV value (~1.76) at 90–100 min post injection and decrease gradually (Figure 2a). In contrast, the peak (SUV value ~ 0.58) appeared at 30–40 min post injection after $^{18}$F-TZ8110 injections, and declined relatively rapidly (Figure 2b). In addition, low

tracer uptake in cerebellum was observed for both tracers, suggesting the feasibility of using cerebellum as the reference region for tracer kinetic modeling analysis.

Further quantitative microPET analyses were carried out for trace kinetic comparison of the two PDE10A radioligands, using 0–120 min data for all scans. Reference based modeling methods have been validated for quantitative PET analysis of PDE10A radioligands in NHPs and humans.[20,22,28,31] Non-displaceable binding potential ($BP_{ND}$) is the typical measurement from reference tissue methods, which refers to the ratio at pseudoequilibrium of specifically bound radioligand to that of nondisplaceable radioligand in tissue.[33] R1 is a measure of radioligand delivery to tissue relative to reference region.[34] Parameters $k_2$, $k_3$, and $k_4$ are rate constants. $k_2$ ($min^{-1}$) represents the efflux of radiotracer through the blood-brain barrier (BBB) by diffusion. The rate constants $k_3$ ($min^{-1}$) and $k_4$ ($min^{-1}$) correspond to the transfer of radioligand between the compartment for nondisplaceable binding ($C_{ND}$) and the compartment for specific binding ($C_B$).[35] The radio of $k_3/k_4$ equals to $BP_{ND}$ value. In the current study, both Logan graphic analysis (LoganREF) and reference tissue model (RTM) yielded similar striatal $BP_{ND}$ with cerebellum as the reference ($^{18}$F-TZ19106B: $BP_{ND}$-LoganREF = 4.36 ± 0.91 vs $BP_{ND}$-RTM = 4.70 ± 0.64; $^{18}$F-TZ8110: $BP_{ND}$-LoganREF = 2.02 ± 0.70 vs $BP_{ND}$-RTM = 2.15 ± 0.66, Table 1). $BP_{ND}$ values from Logan REF strongly correlated with those using RTM (Figure 3). Moreover, RTM revealed similar R1 and $k_2$ values for both tracers ($^{18}$F-TZ19106B: R1 = 0.85 ± 0.16, $k_2$ = 0.059 ± 0.008 $min^{-1}$; $^{18}$F-TZ8110: R1 = 0.89 ± 0.05, $k_2$ = 0.058 ± 0.004 $min^{-1}$, Table 1), while $k_3$ and $k_4$ values significantly differ between the two radiotracers. $^{18}$F-TZ19106B has higher $k_3$ value (0.052 ± 0.008 $min^{-1}$ vs 0.041 ± 0.009 $min^{-1}$) and lower $k_4$ value (0.011 ± 0.002 $min^{-1}$ vs 0.020 ± 0.003 $min^{-1}$) than $^{18}$F-TZ8110 (Table 1). These data suggest that the influx and efflux of both radioligands through BBB are similar; $^{18}$F-TZ19106B has faster transfer rate from $C_{ND}$ to $C_B$ ($k_3$) and slower transfer rate from $C_B$ to $C_{ND}$ ($k4$), compared to $^{18}$F-TZ8110. Accordingly, the difference in $k_3$ and $k_4$ values mainly contribute to higher $BP_{ND}$ value of $^{18}$F-TZ19106B than $^{18}$F-TZ8110.

In addition, to establish the time dependence of $BP_{ND}$ estimates, striatal $BP_{ND}$ values were estimated by LoganREF and RTM using PET data acquiring from 0 to120 min recordings and 0 to 100- and 80 min truncation, and with exclusion of the first 40 min from the Logan linearization (Table 2). The result showed both $^{18}$F-TZ19106B and $^{18}$F-TZ8110 have good time stability of striatal $BP_{ND}$ values, at least up to 80 min of the scan duration. For $^{18}$F-TZ19106B, $BP_{ND}$-LoganREF were 4.36 ± 0.91, 4.40 ± 0.89, 4.40 ± 0.92 using 120, 100, and 80 min data, and $BP_{ND}$-RTM were 4.70 ± 0.64, 4.76 ± 0.77, 4.83 ± 0.76, respectively. The striatal $BP_{ND}$ estimates of 18F-TZ8110 using 120, 100, and 80 min data were 2.02 ± 0.70, 2.06 ± 0.67, 1.95 ± 0.68 (LoganREF), and 2.15 ± 0.66, 2.17 ± 0.72, 2.12 ± 0.81 (RTM).

## Blocking and Displacement Study of $^{18}$F-TZ19106B

Based on the baseline comparison data, $^{18}$F-TZ19106B showed higher striatal retention and favorable tracer kinetics than $^{18}$F-TZ8110. Therefore, we continued further pharmacological characterization of $^{18}$F-TZ19106B in nonhuman primates. As shown in Figure 4, pretreatment with a PDE10A selective inhibitor MP-10 significantly decreased striatal

uptake of $^{18}$F-TZ19106B, suggesting the binding of $^{18}$F-TZ19106B is specific to PDE10A. Furthermore, we also demonstrated sensitivity of $^{18}$F-TZ19106B binding to varying number of available specific binding sites with escalating doses of MP-10 blockade (0.3, 0.5, 1.0, 1.5, and 2.0 mg/kg). The resulting $BP_{ND}$ values were 2.93, 1.76, 1.06, 0.46, and 0.48 by Logan REF and 2.96, 1.62, 0.94, 0.52, and 0.45 by RTM (Table 3). Target (PDE10A in the striatum) occupancy levels then were calculated as the relative change in striatal $BP_{ND}$ using either LoganREF or RTM; and it refers to the percentage of the enzyme PDE10A binding sites bound by the unlabeled drug molecule (MP-10). Accordingly, MP-10 pretreatment doses of 0.3, 0.5, 1.0, 1.5, and 2.0 mg/kg produced occupancy levels of 33%, 60%, 76%, 89%, 89% determined by Logan REF, and 35%, 64%, 79%, 89%, 90% by RTM (Table 3).

Reversibility of radioligand binding is important to consider in the application of tracer kinetic models.[36] Thus, we administered unlabeled MP-10 2.0 mg/kg 40 min post injection of $^{18}$F-TZ19106B to determine reversibility of the binding of $^{18}$F-TZ19106B to PDE10A. As shown in Figure 5, striatal uptake declined tremendously after injection of MP-10, while the radiotracer uptake in cerebellum was not obviously impacted, indicating a specific and reversible binding of $^{18}$F-TZ19106B to PDE10A.

## Eticlopride Pretreatment Study Using $^{18}$F-TZ19106B

Emerging evidence suggests that PDE10A play a key role in regulation of striatal signaling which involve dopaminergic pathways and cAMP-dependent pathways. Reduced striatal PDE10A and dopaminergic D2 receptor levels were detected by 18F-MNI-659/$^{11}$C-raclopride PET or 3H-AMG-7980/$^{3}$H-raclopride autoradiography in the same set of Huntington Disease (HD) model mice (zQ175 and R6/2).[37,38] A recent clinical study further revealed that D2 receptor and PDE10A availability, indicated by striatal uptake of $^{18}$F-MNI-659 and $^{11}$C-raclopride, were 62 ± 12%, and 21 ± 33% of control values ($p < 0.05$) in stage 1 HD gene expansion carriers (HDGECs), and 72 ± 12% and 53 ± 22% of control values in in premanifest HDGECs.[39] In a longitudinal microPET study with $^{18}$F-JNJ42259152, repeated stimulation of the dopamine neuro-transmission by D-amphetamine significantly increased in vivo PDE10A binding in normal rat striatum, while chronic treatment with the selective D1 antagonist SCH23390 decreased PDE10A striatal binding.[40] In our study, acute pretreatment with (−)-eticlopride (0.025 mg/kg), a selective D2 antagonist, increased the striatal uptake of $^{18}$F-TZ19106B by 44% ($BP_{ND}$-LoganREF) or 34% ($BP_{ND}$-RTM). This funding was consistent with Dlaboga's report which used quantitative immunoblot analysis to quantify PDE10A expression after treatment with haloperidol, a selective D2/3 receptor antagonist. A significant increase in PDE10A expression was detected after a 21-day treatment of rats with haloperidol.[41] Based on our data and others', the potential interaction between PDE10A pathway and dopaminergic signaling was summarized as shown in Figure 6. Intercellular cAMP levels in MSNs is modulated by adenylate cyclase and PDE10A. Adenylate cyclase, the enzyme that catalyzes the conversion of ATP to cAMP, is activated by D1 signaling and suppressed by D2 signaling. Concordantly, D2 inhibition induced by (−)-eticlopride removes suppression of adenylate cyclase, thereby increasing cAMP levels, which lead to compensatory upregulation of PDE10A to hydrolyze overexpressed cAMP. In agreement with our hypothesis, increased in vivo cAMP level causes upregulation of PDE10A $BP_{ND}$ in rat

striatum, measured by $^{18}$F-JNJ42259152 microPET.[42] Since modulation of cAMP levels could have therapeutic benefits for a broad range of neuropsychiatric disorders,[43] PDE10A levels by PET measures may be used as a (indirect) functional readout of novel antipsychotic therapies enhancing cAMP levels.

In summary, quantitative comparison of $^{18}$F-TZ19106B and $^{18}$F-TZ8110 in in vivo imaging PDE10A were conducted in nonhuman primates via PET. The data showed that $^{18}$F-TZ19106B had higher striatal uptake and tracer retention in NHP brains than 18F-TZ8110. Reference-based modeling analysis revealed that both tracers showed good time stability of striatal $BP_{ND}$, while $^{18}$F-TZ19106B has higher $BP_{ND}$, larger $k_3$ value and smaller $k_4$ value compared to $^{18}$F-TZ8110. Thus $^{18}$F-TZ19106B was further characterized pharmacologically. Blocking and displacement studies with MP-10 suggest specific and reversible binding of $^{18}$F-TZ19106B to PDE10A. Pretreatment with (−)-eticlopride upregulated the striatal uptake of $^{18}$F-TZ19106B, indicating PET with a suitable PDE10A radioligand is not only useful for determining target engagement of PDE10A inhibitors, but also may serve as a tool to evaluate the effect of novel antipsychotic drugs. $^{18}$F-TZ19106B has high striatal retention over the 3h scan period in NHP brains, which may permit measurements for static scan acquisition with good consistency, but not for short-term dynamic scans post injection of radiotracers. The toxic evaluation of $^{18}$F-TZ19106B counterpart cold standard is in the process. We are planning to seek United States Food and Drug Administration (FDA) approval for human use of this radiotracer, then to perform translational clinical investigation in human subjects.

## METHODS

### Radiochemical Synthesis

The radiosyntheses of $^{18}$F-TZ19106B and 18F-TZ8110 were accomplished by a two-step procedure as reported recently by our group.[32] First, ethylene ditosylate was reacted with $^{18}$F-KF/Kryptofix 2.2.2 in acetonitrile (ACN) and then purified on a reversed phase HPLC system to afford $^{18}$F-fluoroethyl tosylate with a 60–75% radiochemical yield. Second, nucleophilic substitution of corresponding phenol precursors with $^{18}$F-fluoroethyl tosylate in dimethyl sulfoxide (DMSO) followed by purifying on reversed phase HPLC afforded $^{18}$F-TZ19106B and $^{18}$F-TZ8110 in 65–72% and 30–35% radiochemical yield, respectively. The two-step radiosynthesis took 3 h, and both tracers have high specific activity > 74 GBq/$\mu$mol (decay corrected to EOS) and high radiochemical purity > 98%.

### Animals

All animal experiments were performed following the Guidelines for the Care and Use of Research Animals under a research protocol approved by Washington University Institutional Animal Care and Use Committee. This work was conducted in nonhuman primate microPET facility at the Washington University School of Medicine in St. Louis.

PET imaging studies were carried out on adult male *Macaca fascicularis*, $n$ = 5, weighing 7–8 kg. We collected five or six baseline scans in three NHPs for each radiotracer, and each scan lasted for 120 or 180 min. A same animal was used for pretreatment and displacement

studies. Animals were prepared for microPET studies as previously reported.[30–32,44] 1.5–2.5% isoflurane inhalation anesthesia was maintained throughout the microPET imaging sessions. A 20-gauge plastic catheter was inserted into a limb vein to permit hydration and injection of the radiotracer. For the same animal, the interval between two consecutive PET scans was at least 2 weeks.

### MicroPET Data Acquisition

The microPET studies were done using a MicroPET Focus 220 scanner (Concorde/CTI/Siemens Microsystems, Knoxville, TN). Prior to each PET acquisition, a 45 min transmission scan for attenuation correction was done. Subsequently, 185–370 MBq of $^{18}$F-TZ19106B and $^{18}$F-TZ8110 was intravenously injected, and a 120 min dynamic (3× 1 min frames, 4× 2 min frames, 3× 3 min frames, and 20× 5 min frames) or a 180 min dynamic (3× 1 min frames, 4× 2 min frames, 3× 3 min frames, and 32× 5 min frames) PET scan was acquired. Pretreatment studies were performed by intravenous injection of either MP-10 (0.3, 0.5, 1.0, 1.5, and 2.0 mg/kg) or (−)-eticlopride (0.025 mg/kg) 5 min prior to the radiotracer injection. For the displacement study, 2.0 mg/kg MP-10 was intravenously injected at 40 min after injection of the radiotracer.

### PET Image Processing

The PET/CT images were processed according to our published procedure.[31,44] Briefly, sinogram data were corrected for attenuation, random and scatter, and reconstructed using filtered back projection.[45] The final reconstructed resolution was 2.00 mm full width at half-maximum (fwhm) for all three dimensions (axial) at center of the field of view. The reconstructed PET images was coregistered with magnetization-prepared rapid gradient echo (MP-RAGE) MR images using Automated Image Registration (AIR),[46] and superimposed using Analyze 10.0 (AnalyzeDirect, Overland Park, KS). For quantitative analyses, a program VIDI that was coded by our PET imaging analysts and routinely used in our institute for PET data processing[47,48] was used. Regions of interest (ROIs) were manually drawn on MRI images for striatum and cerebellum, and transformed into PET images using the coregistration transformation matrix. The ROIs for each animal were identified on a baseline scan and kept fixed for all subsequent studies. Time-activity curves (TACs) were then obtained from the dynamic PET images. Activity measures were calculated and standardized to the body weight and the injected dose of radioactivity, and yield standardized uptake values (SUVs). To minimize noise signal in the presentation, data in TAC graphics have been smoothed by “LOWESS” using GraphPad Prism 6.0 (GraphPad Software, Inc., San Diego, CA), while tracer kinetic analysis was based on original data without smoothing.

### Reference Based Tracer Kinetic Modeling

To quantitatively evaluate the kinetic property of each radioligand, LoganREF and RTM were carried out for kinetics modeling. LoganREF is a wide used reference-based graphical method.[49] LoganREF is able to provide highly correlated BP estimates compared with compartmental tracer kinetic models with blood input function; this method has simplified computation and is straightforward.[50] RTM is a compartmental modeling approach that used the reference tissue time activity curve as input.[51] Compared to graphical analysis, the

reference tissue model can extract more physiological information from measured tracer kinetics.[50] Furthermore, the use of higher order reference tissue models (such as RTM vs simplified reference tissue model (SRTM)), has been proposed to reduce the bias of BP or distribution volume ratio (DVR) of target tissue to reference tissue estimates.[50] Therefore, LoganREF and RTM were chosen for tracer kinetic modeling in the current study as an initial phase for evaluating the two radiotracers. The binding potential was defined as a ratio of specifically bound ligand to its free concentration. $BP_{ND}$ was calculated from DVR using the term: $BP_{ND}$ = DVR-1.[33] R1, $k_{2,}$ $k_3$, and $k_4$ values were also obtained from the RTM model.[52,53] Target occupancy levels ($Occ^M$) were calculated as the relative change in striatal $BP_{ND}$ using either LoganREF or RTM, as follow: $Occ^M$ = ($BP_{ND}$-baseline − $BP_{ND}$-pretreatment)/$BP_{ND}$-baseline × 100%.

## Acknowledgments

The authors like to thank the Cyclotron Facility of Washington University for providing [$^{18}$F]fluoride. We would also like to thank John Hood, Emily William, Darryl Craig, and Christina Zukas for their assistance with NHP microPET scans.

**Funding**

This work was supported by NIH/NIMH (MH092797); NIH/NINDS&NIA (NS061025, NS103957; NS075527, NS103988, NS058714, NS075321, NS103957, and U54TR001456); DOE training grants (DESC0008432 and DESC0012737); American Parkinson Disease Association (APDA) Center for Advanced PD Research at Washington University; Greater St. Louis Chapter of the APDA; McDonnell Center for Higher Brain Function; Barnes-Jewish Hospital Foundation (Elliot Stein Family Fund and Parkinson Disease Research Fund).

## ABBREVIATIONS

| | |
|---|---|
| **AIR** | Automated Image Registration |
| **BBB** | blood-brain barrier |
| **BP** | binding potential |
| **$BP_{ND}$** | nondisplaceable binding potential |
| **cAMP** | cyclic adenosine monophosphate |
| **$C_B$** | compartment for specific binding |
| **$C_{ND}$** | compartment for nondisplaceable binding |
| **DA** | dopaminergic |
| **DARPP-32** | dopamine- and cAMP-regulated neuronal phosphoprotein |
| **DVR** | distribution volume ratio |
| **fwhm** | full width at half-maximum |
| **HD** | Huntington disease |
| **HDGECs** | HD gene expansion carriers |
| **LoganREF** | Logan graphic analysis |

| | |
|---|---|
| **MSNs** | medium spiny neurons |
| **NHPs** | nonhuman primates |
| **NLSF** | nonlinear least-squares fitting |
| **$Occ^M$** | target occupancy levels |
| **PDE10A** | phosphodiesterase 10A |
| **PKA** | protein kinase A |
| **ROIs** | regions of interest |
| **RTM** | reference tissue model |
| **SUVs** | standardized uptake values |
| **TACs** | time–activity curves |

## References


1. Kotera J, Fujishige K, Yuasa K, Omori K. Characterization and phosphorylation of PDE10A2, a novel alternative splice variant of human phosphodiesterase that hydrolyzes cAMP and cGMP. Biochem Biophys Res Commun. 1999; 261:551–557. [PubMed: 10441464]
2. Nishi A, Kuroiwa M, Miller DB, O'Callaghan JP, Bateup HS, Shuto T, Sotogaku N, Fukuda T, Heintz N, Greengard P, Snyder GL. Distinct Roles of PDE4 and PDE10A in the Regulation of cAMP/PKA Signaling in the Striatum. J Neurosci. 2008; 28:10460–10471. [PubMed: 18923023]
3. Xie Z, Adamowicz WO, Eldred WD, Jakowski AB, Kleiman RJ, Morton DG, Stephenson DT, Strick CA, Williams RD, Menniti FS. Cellular and subcellular localization of PDE10A, a striatum-enriched phosphodiesterase. Neuroscience. 2006; 139:597–607. [PubMed: 16483723]
4. Sano H, Nagai Y, Miyakawa T, Shigemoto R, Yokoi M. Increased social interaction in mice deficient of the striatal medium spiny neuron-specific phosphodiesterase 10A2. J Neurochem. 2008; 105:546–556. [PubMed: 18088367]
5. Kotera J, Sasaki T, Kobayashi T, Fujishige K, Yamashita Y, Omori K. Subcellular localization of cyclic nucleotide phosphodiesterase type 10A variants, and alteration of the localization by cAMP-dependent protein kinase-dependent phosphorylation. J Biol Chem. 2004; 279:4366–4375. [PubMed: 14604994]
6. Nishi A, Snyder GL, Greengard P. Bidirectional regulation of DARPP-32 phosphorylation by dopamine. J Neurosci. 1997; 17:8147–8155. [PubMed: 9334390]
7. Charych EI, Jiang LX, Lo F, Sullivan K, Brandon NJ. Interplay of Palmitoylation and Phosphorylation in the Trafficking and Localization of Phosphodiesterase 10A: Implications for the Treatment of Schizophrenia. J Neurosci. 2010; 30:9027–9037. [PubMed: 20610737]
8. Giorgi M, Melchiorri G, Nuccetelli V, D'Angelo V, Martorana A, Sorge R, Castelli V, Bernardi G, Sancesario G. PDE10A and PDE10A-dependent cAMP catabolism are dysregulated oppositely in striatum and nucleus accumbens after lesion of midbrain dopamine neurons in rat: A key step in parkinsonism physiopathology. Neurobiol Dis. 2011; 43:293–303. [PubMed: 21515371]
9. Megens AAHP, Hendrickx HMR, Hens KA, Fonteyn I, Langlois X, Lenaerts I, Somers MVF, de Boer P, Vanhoof G. Pharmacology of JNJ-42314415, a Centrally Active Phosphodiesterase 10A (PDE10A) Inhibitor: A Comparison of PDE10A Inhibitors with D-2 Receptor Blockers as Potential Antipsychotic Drugs. J Pharmacol Exp Ther. 2014; 349:138–154. [PubMed: 24421319]
10. Nishi A, Kuroiwa M, Shuto T. Mechanisms for the modulation of dopamine D-1 receptor signaling in striatal neurons. Front Neuroanat. 2011; 5:43. [PubMed: 21811441]

11. Threlfell S, Sammut S, Menniti FS, Schmidt CJ, West AR. Inhibition of Phosphodiesterase 10A Increases the Responsiveness of Striatal Projection Neurons to Cortical Stimulation. J Pharmacol Exp Ther. 2009; 328:785–795. [PubMed: 19056933]
12. Bateup HS, Svenningsson P, Kuroiwa M, Gong S, Nishi A, Heintz N, Greengard P. Cell type-specific regulation of DARPP-32 phosphorylation by psychostimulant and antipsychotic drugs. Nat Neurosci. 2008; 11:932–939. [PubMed: 18622401]
13. Tu Z, Xu JB, Jones LA, Li SH, Mach RH. Carbon-11 labeled papaverine as a PET tracer for imaging PDE10A: radiosynthesis, in vitro and in vivo evaluation. Nucl Med Biol. 2010; 37:509–516. [PubMed: 20447563]
14. Celen S, Koole M, Ooms M, De Angelis M, Sannen I, Cornelis J, Alcazar J, Schmidt M, Verbruggen A, Langlois X, Van Laere K, Andres JI, Bormans G. Preclinical evaluation of [F-18]JNJ42259152 as a PET tracer for PDE10A. NeuroImage. 2013; 82:13–22. [PubMed: 23664955]
15. Ahmad R, Bourgeois S, Postnov A, Schmidt ME, Bormans G, Van Laere K, Vandenberghe W. PET imaging shows loss of striatal PDE10A in patients with Huntington disease. Neurology. 2014; 82:279–281. [PubMed: 24353339]
16. Plisson C, Weinzimmer D, Jakobsen S, Natesan S, Salinas C, Lin SF, Labaree D, Zheng MQ, Nabulsi N, Marques TR, Kapur S, Kawanishi E, Saijo T, Gunn RN, Carson RE, Rabiner EA. Phosphodiesterase 10A PET Radioligand Development Program: From Pig to Human. J Nucl Med. 2014; 55:595–601. [PubMed: 24614221]
17. Niccolini F, Foltynie T, Marques TR, Muhlert N, Tziortzi AC, Searle GE, Natesan S, Kapur S, Rabiner EA, Gunn RN, Piccini P, Politis M. Loss of phosphodiesterase 10A expression is associated with progression and severity in Parkinson's disease. Brain. 2015; 138:3003–3015. [PubMed: 26210536]
18. Marques TR, Natesan S, Niccolini F, Politis M, Gunn RN, Searle GE, Howes O, Rabiner EA, Kapur S. Phosphodiesterase 10A in Schizophrenia: A PET Study Using [C-11]IMA107. Am J Psychiatry. 2016; 173:714–721. [PubMed: 26892941]
19. Niccolini F, Haider S, Marques TR, Muhlert N, Tziortzi AC, Searle GE, Natesan S, Piccini P, Kapur S, Rabiner EA, Gunn RN, Tabrizi SJ, Politis M. Altered PDE10A expression detectable early before symptomatic onset in Huntington's disease. Brain. 2015; 138:3016–3029. [PubMed: 26198591]
20. Kehler J, Kilburn JP, Estrada S, Christensen SR, Wall A, Thibblin A, Lubberink M, Bundgaard C, Brennum LT, Steiniger-Brach B, Christoffersen CT, Timmermann S, Kreilgaard M, Antoni G, Bang-Andersen B, Nielsen J. Discovery and Development of C-11-Lu AE92686 as a Radioligand for PET Imaging of Phosphodiesterase10A in the Brain. J Nucl Med. 2014; 55:1513–1518. [PubMed: 24994928]
21. Boden R, Persson J, Wall A, Lubberink M, Ekselius L, Larsson EM, Antoni G. Striatal phosphodiesterase 10A and medial prefrontal cortical thickness in patients with schizophrenia: a PET and MRI study. Transl Psychiatry. 2017; 7:e1050. [PubMed: 28267149]
22. Barret O, Thomae D, Tavares A, Alagille D, Papin C, Waterhouse R, McCarthy T, Jennings D, Marek K, Russell D, Seibyl J, Tamagnan G. Vivo Assessment and Dosimetry of 2 Novel PDE10A PET Radiotracers in Humans: F-18-MNI-659 and F-18-MNI-654. J Nucl Med. 2014; 55:1297–1304. [PubMed: 24898025]
23. Russell DS, Jennings DL, Barret O, Tamagnan GD, Alagille D, Seibyl JP, Marek KL. Striatal PDE10 expression in Parkinson's disease (PD) and healthy controls using [F-18]MNI-659 PET imaging. Movement Disord. 2016; 31:S282–S282.
24. Russell DS, Barret O, Jennings DL, Friedman JH, Tamagnan GD, Thomae D, Alagille D, Morley TJ, Papin C, Papapetropoulos S, Waterhouse RN, Seibyl JP, Marek KL. The Phosphodiesterase 10 Positron Emission Tomography Tracer, [F-18]MNI-659, as a Novel Biomarker for Early Huntington Disease. Jama Neurol. 2014; 71:1520–1528. [PubMed: 25322077]
25. Russell DS, Jennings DL, Barret O, Tamagnan GD, Carroll VM, Caille F, Alagille D, Morley TJ, Papin C, Seibyl JP, Marek KL. Change in PDE10 across early Huntington disease assessed by [F-18]MNI-659 and PET imaging. Neurology. 2016; 86:748–754. [PubMed: 26802091]
26. Takano A, Stenkrona P, Stepanov V, Amini N, Martinsson S, Tsai M, Goldsmith P, Xie JH, Wu JT, Uz T, Halldin C, Macek TA. A human [C-11]T-773 PET study of PDE10A binding after oral

administration of TAK-063, a PDE10A inhibitor. NeuroImage. 2016; 141:10–17. [PubMed: 27423256]

27. Tu Z, Fan JD, Li SH, Jones LA, Cui JQ, Padakanti PK, Xu JB, Zeng DX, Shoghi KI, Perlmutter JS, Mach RH. Radiosynthesis and in vivo evaluation of [C-11]MP-10 as a PET probe for imaging PDE10A in rodent and non-human primate brain. Bioorg Med Chem. 2011; 19:1666–1673. [PubMed: 21315609]
28. Lin SF, Labaree D, Chen MK, Holden D, Gallezot JD, Kapinos M, Teng JK, Najafzadeh S, Plisson C, Rabiner EA, Gunn RN, Carson RE, Huang YY. Further Evaluation of [C-11]MP-10 as a Radiotracer for Phosphodiesterase 10A: PET Imaging Study in Rhesus Monkeys and Brain Tissue Metabolite Analysis. Synapse. 2015; 69:86–95. [PubMed: 25450608]
29. Li JF, Jin HJ, Zhou HY, Rothfuss J, Tu ZD. Synthesis and in vitro biological evaluation of pyrazole group-containing analogues for PDE10A. MedChemComm. 2013; 4:443–449. [PubMed: 23585921]
30. Fan JD, Zhang X, Li JF, Jin HJ, Padakanti PK, Jones LA, Flores HP, Su Y, Perlmutter JS, Tu ZD. Radiosyntheses and in vivo evaluation of carbon-11 PET tracers for PDE10A in the brain of rodent and nonhuman primate. Bioorg Med Chem. 2014; 22:2648–2654. [PubMed: 24721831]
31. Liu H, Jin HJ, Yue XY, Zhang X, Yang H, Li JF, Flores H, Su Y, Perlmutter JS, Tu ZD. Preclinical evaluation of a promising C-11 labeled PET tracer for imaging phosphodiesterase 10A in the brain of living subject. NeuroImage. 2015; 121:253–262. [PubMed: 26216275]
32. Li JF, Zhang X, Jin HJ, Fan JD, Flores H, Perlmutter JS, Tu ZD. Synthesis of Fluorine-Containing Phosphodiesterase 10A (PDE10A) Inhibitors and the In Vivo Evaluation of F-18 Labeled PDE10A PET Tracers in Rodent and Nonhuman Primate. J Med Chem. 2015; 58:8584–8600. [PubMed: 26430878]
33. Innis RB, Cunningham VJ, Delforge J, Fujita M, Gjedde A, Gunn RN, Holden J, Houle S, Huang SC, Ichise M, Iida H, Ito H, Kimura Y, Koeppe RA, Knudsen GM, Knuuti J, Lammertsma AA, Laruelle M, Logan J, Maguire RP, Mintun MA, Morris ED, Parsey R, Price JC, Slifstein M, Sossi V, Suhara T, Votaw JR, Wong DF, Carson RE. Consensus nomenclature for in vivo imaging of reversibly binding radioligands. J Cereb Blood Flow Metab. 2007; 27:1533–1539. [PubMed: 17519979]
34. Ichise M, Liow JS, Lu JQ, Takano T, Model K, Toyama H, Suhara T, Suzuki T, Innis RB, Carson TE. Linearized reference tissue parametric Imaging methods: Application to [C-11]DASB positron emission tomography studies of the serotonin transporter in human brain. J Cereb Blood Flow Metab. 2003; 23:1096–1112. [PubMed: 12973026]
35. Cselényi Z, Jönhagen ME, Forsberg A, Halldin C, Julin P, Schou M, Johnström P, Varnäs K, Svensson S, Farde L. Clinical Validation of $^{18}$F-AZD4694, an Amyloid-$\beta$–Specific PET Radioligand. J Nucl Med. 2012; 53:415–424. [PubMed: 22323782]
36. Ichise, M. Neuroreceptor Imaging and Kinetic Modeling. In: Van Heertum, RL.Tikofsky, RS., Ichise, M., editors. Functional Cerebral SPECT and PET Imaging. 4th. Lippincott Williams & Wilkins; Philadelphia: 2009. p. 40-53.
37. Haggkvist J, Toth M, Tari L, Varnas K, Svedberg M, Forsberg A, Nag S, Dominguez C, Munoz-Sanjuan I, Bard J, Wityak J, Varrone A, Halldin C, Mrzljak L. Longitudinal Small-Animal PET Imaging of the zQ175 Mouse Model of Huntington Disease Shows In Vivo Changes of Molecular Targets in the Striatum and Cerebral Cortex. J Nucl Med. 2017; 58:617–622. [PubMed: 27856625]
38. Miller S, Hill della Puppa G, Reidling J, Marcora E, Thompson LM, Treanor J. Comparison of Phosphodiesterase 10A, Dopamine Receptors D1 and D2 and Dopamine Transporter Ligand Binding in the Striatum of the R6/2 and BACHD Mouse Models of Huntington's Disease. J Huntington's Dis. 2014; 3:333–341. [PubMed: 25575954]
39. Fazio P, Fitzer-Attas C, Mrzljak L, Martinsson S, Landwehrmeyer G, Bronzova J, Al-Tawil N, Halldin C, Sampaio C, Varrone A. E31 Positron Emission Tomography Imaging Of Phosphodiesterase 10 A Enzyme And Dopamine D2 Receptor In Huntingtoń s Disease Gene Expansion Carriers, Journal of Neurology. J Neurol, Neurosurg Psychiatry. 2014; 85:A47–A47.
40. Ooms M, Celen S, De Hoogt R, Lenaerts I, Liebregts J, Vanhoof G, Langlois X, Postnov A, Koole M, Verbruggen A, Van Laere K, Bormans G. Striatal phosphodiesterase 10A availability is altered secondary to chronic changes in dopamine neurotransmission. EJNMMI Radiopharm Chem. 2017; 1:3. [PubMed: 29564380]

41. Dlaboga D, Hajjhussein H, O'Donnell JM. Chronic haloperidol and clozapine produce different patterns of effects on phosphodiesterase-1B,-4B, and-10A expression in rat striatum. Neuropharmacology. 2008; 54:745–754. [PubMed: 18222493]
42. Ooms M, Attili B, Celen S, Koole M, Verbruggen A, Van Laere K, Bormans G. [$^{18}$F]JNJ42259152 binding to phosphodiesterase 10A, a key regulator of medium spiny neuron excitability, is altered in the presence of cyclic AMP. J Neurochem. 2016; 139:897–906. [PubMed: 27664396]
43. Garcia AM, Martinez A, Gil C. Enhancing cAMP Levels as Strategy for the Treatment of Neuropsychiatric Disorders. Curr Top Med Chem. 2016; 16:3527–3535. [PubMed: 27112214]
44. Liu H, Jin H, Yue X, Han J, Yang H, Flores H, Su Y, Alagille D, Perlmutter JS, Tamagnan G, Tu Z. Comparison of [$^{11}$C]TZ1964B and [$^{18}$F]MNI659 for PET imaging brain PDE10A in nonhuman primates, Pharmacol Res. Perspect 4. Pharmacol Res Perspect. 2016; 4:e00253. [PubMed: 27713824]
45. Miller TR, Wallis JW, Wilson AD. Interactive Reconstruction in Single-Photon Tomography. Eur J Nucl Med. 1989; 15:189–193. [PubMed: 2787746]
46. Woods RP, Mazziotta JC, Cherry SR. Mri-Pet Registration with Automated Algorithm. J Comput Assisted Tomogr. 1993; 17:536–546.
47. Jin H, Yue X, Liu H, Han J, Flores H, Su Y, Parsons SM, Perlmutter JS, Tu Z. Kinetic modeling of [$^{18}$F]VAT, a novel radioligand for PET imaging vesicular acetylcholine transporter (VAChT) in nonhuman primate brain. J Neurochem. 2018; doi: 10.1111/jnc.14291
48. Jin H, Zhang X, Yue X, Liu H, Li J, Yang H, Flores H, Su Y, Parsons SM, Perlmutter JS, Tu Z. Kinetics modeling and occupancy studies of a novel C-11 PET tracer for VAChT in nonhuman primates. Nucl Med Biol. 2016; 43:131–139. [PubMed: 26872437]
49. Logan J, Fowler JS, Volkow ND, Wang GJ, Ding YS, Alexoff DL. Distribution volume ratios without blood sampling from graphical analysis of PET data. J Cereb Blood Flow Metab. 1996; 16:834–840. [PubMed: 8784228]
50. Zhou Y, Resnick SM, Ye WG, Fan H, Holt DP, Klunk WE, Mathis CA, Dannals R, Wong DF. Using a reference tissue model with spatial constraint to quantify [C-11]Pittsburgh compound BPET for early diagnosis of Alzheimer's disease. NeuroImage. 2007; 36:298–312. [PubMed: 17449282]
51. Cunningham VJ, Hume SP, Price GR, Ahier RG, Cremer JE, Jones AK. Compartmental analysis of diprenorphine binding to opiate receptors in the rat in vivo and its comparison with equilibrium data in vitro. J Cereb Blood Flow Metab. 1991; 11:1–9. [PubMed: 1845764]
52. Lammertsma AA, Hume SP. Simplified reference tissue model for PET receptor studies. NeuroImage. 1996; 4:153–158. [PubMed: 9345505]
53. Watabe H, Itoh M, Cunningham V, Lammertsma AA, Bloomfield P, Mejia M, Fujiwara T, Jones AKP, Jones T, Nakamura T. Noninvasive quantification of rCBF using positron emission tomography. J Cereb Blood Flow Metab. 1996; 16:311–319. [PubMed: 8594064]

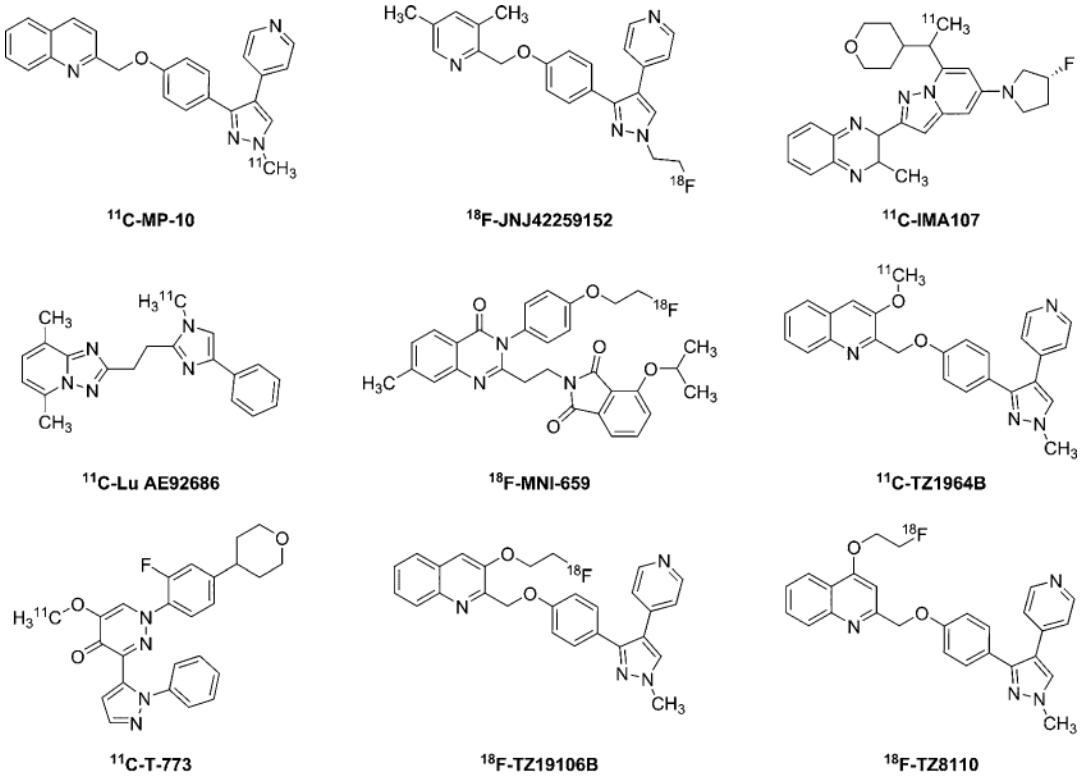


**Figure 1.**
Chemical structures of leading PDE10A radioligands.

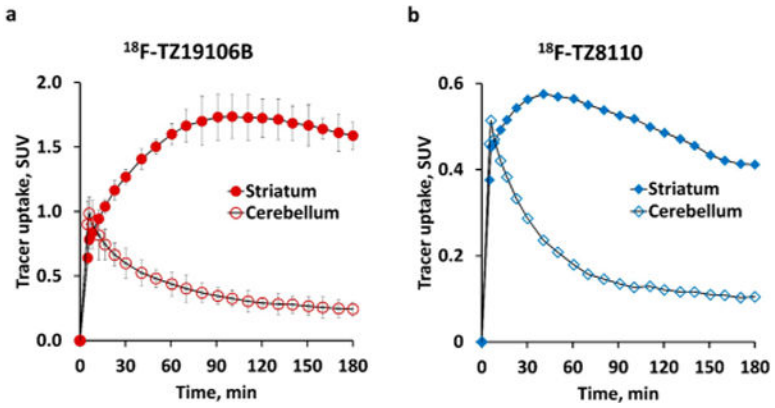


**Figure 2.**

Time–activity curves (TACs) of microPET in NHP brains using two PDE10A radioligands $^{18}$F-TZ19106B, and $^{18}$F-TZ8110. (a) $^{18}$F-TZ19106B TACs in NHP striatum and cerebellum using averaged SUVs ($n$ = 2 scans), striatum uptake reached the max SUV value (~1.76) at 90–100 min postinjection and decreased gradually; (b) $^{18}$F-TZ8110 TACs in NHP striatum and cerebellum ($n$ = 1 scan), the peak (SUV value ~ 0.58) appeared at 30–40 min postinjection and declined relatively rapidly. Note: To minimize noise signal in the presentation, data in TAC graphics have been smoothed by “LOWESS” using GraphPad Prism 6.0 (GraphPad Software, Inc., San Diego, CA), while tracer kinetic analysis was based on original data without smoothing.

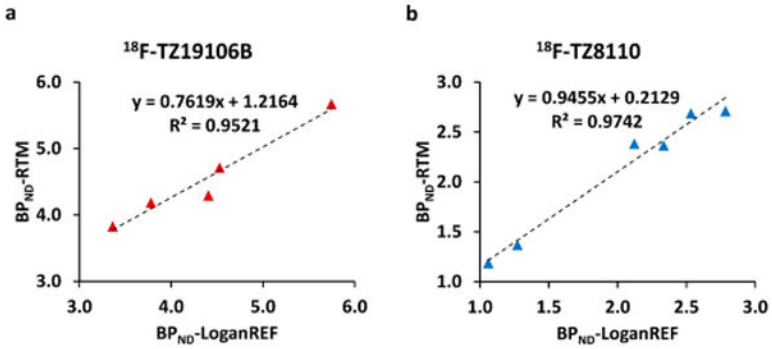


**Figure 3.**

Correlation between $BP_{ND}$-LoganREF and $BP_{ND}$-RTM for $^{18}$F-TZ19106B and $^{18}$F-TZ8110 in NHP striatum. $n$ = 5 scans in 3 NHPs for $^{18}$F-TZ19106B (a), $n$ = 6 scans in 3 NHPs for $^{18}$F-TZ8110 (b). Data from 0 to 120 min post-tracer injection were used for $BP_{ND}$ estimates. $BP_{ND}$-LoganREF values of both tracers strongly correlated with $BP_{ND}$-RTM values.

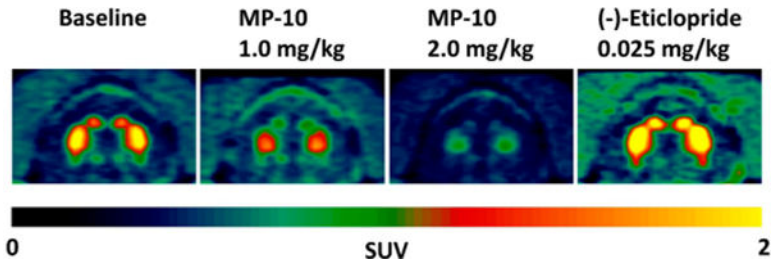


**Figure 4.**

Representative $^{18}$F-TZ19106B microPET images of NHP brain. High striatum uptake at baseline was blocked by pretreatments with 1.0 or 2.0 mg/kg MP-10, a specific PDE10A inhibitor. In contrast, pretreatment with (−)-eticlopride even increased the striatal uptake of $^{18}$F-TZ19106B. All PET images are summed from 0 to 120 min.

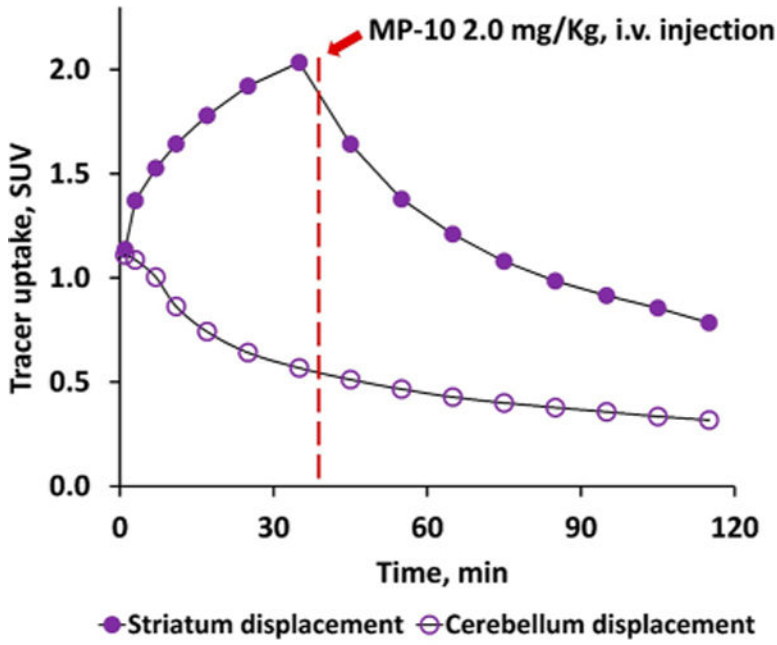


**Figure 5.**

Displacement study of $^{18}$F-TZ19106B in NHP brain. The striatal uptake of 18F-TZ19106B significantly decreased after i.v. injection of MP-10 at 40 min post tracer injection (purple solid circles), while the tracer uptake in the cerebellum was not impacted by the MP-10 injection (purple open circles).

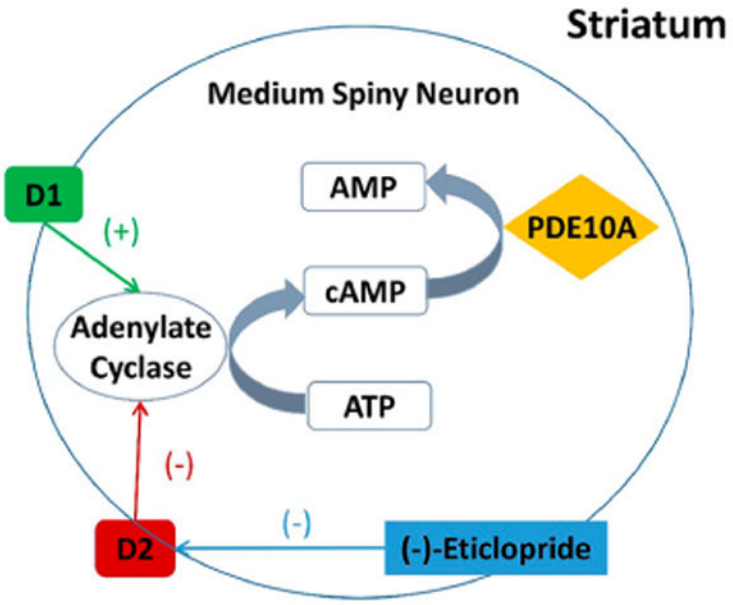


**Figure 6.**

Simplified circuitry cartoon showing the interaction between PDE10A pathway and dopaminergic signaling in medium spiny neurons (MSNs) of striatum. Intercellular cAMP levels in MSNs is modulated by adenylate cyclase and PDE10A. Adenylate cyclase, which catalyzes the conversion of ATP to cAMP, is activated by D1 signaling and suppressed by D2 signaling. Concordantly, D2 inhibition induced by (−)-eticlopride removes the suppression of adenylate cyclase, resulting in increased cAMP levels, which lead to compensatory upregulation of PDE10A to hydrolyze overexpressed cAMP.

**Table 1**

Kinetic Parameters of PET Brain Imaging in NHPs at Baseline Using $^{18}$F-TZ19106B and $^{18}$F-TZ8110

| | LoganREF | RTM | | | | |
|---|---|---|---|---|---|---|
| **tracers** | **$BP_{ND}$** | **R1** | **$k_2$ ($min^{-1}$)** | **$k_3$ ($min^{-1}$)** | **$k_4$ ($min^{-1}$)** | **$BP_{ND}(k_3/k_4)$** |
| $^{18}$F-TZ19106B[a] | 4.36 ± 0.91 | 0.85 ± 0.16 | 0.059 ± 0.008 | 0.052 ± 0.008 | 0.011 ± 0.002 | 4.70 ± 0.64 |
| $^{18}$F-TZ8110[b] | 2.02 ± 0.70 | 0.89 ± 0.05 | 0.058 ± 0.004 | 0.041 ± 0.009 | 0.020 ± 0.003 | 2.15 ± 0.66 |

[a] $n$ = 5 in 3 NHPs.

[b] $n$ = 6 in 3 NHPs.

**Table 2**

Striatal $BP_{ND}$ Estimates of $^{18}$F-TZ19106B and $^{18}$F-TZ8110 Using Different Scan Duration

| radioligand | scan duration for analysis[c] | 120 min | 100 min | 80 min |
|---|---|---|---|---|
| $^{18}$F-TZ19106B[a] | LoganREF | 4.36 ± 0.91 | 4.40 ± 0.89 | 4.40 ± 0.92 |
| | RTM | 4.70 ± 0.64 | 4.76 ± 0.77 | 4.83 ± 0.76 |
| $^{18}$F-TZ8110[b] | LoganREF | 2.02 ± 0.70 | 2.06 ± 0.67 | 1.95 ± 0.68 |
| | RTM | 2.15 ± 0.66 | 2.17 ± 0.72 | 2.12 ± 0.81 |

[a] $n$ = 5 in 3 NHPs.

[b] $n$ = 6 in 3 NHPs.

[c] LoganREF analysis uses data starting from 40 min post injection for both tracers, and RTM uses data starting from 0 min postinjection.

**Table 3**

Binding Potential and Occupancy Levels at Baseline and in Pretreatment Studies of $^{18}$F-TZ19106B PET

| | $BP_{ND}$-LoganREF | $Occ^m$, %[a] | $BP_{ND}$-RTM | $Occ^m$, % |
|---|---|---|---|---|
| baseline (avg) MP-10, mg/kg | 4.36 | | 4.54 | |
| 2.0 | 0.48 | 89.00 | 0.45 | 89.99 |
| 1.5 | 0.46 | 89.40 | 0.52 | 88.61 |
| 1.0 | 1.06 | 75.76 | 0.94 | 79.36 |
| 0.5 | 1.76 | 59.69 | 1.62 | 64.27 |
| 0.3 | 2.93 | 32.81 | 2.96 | 34.86 |
| (−)-eticlopride, 0.025 mg/kg | 6.28 | −44.08 | 6.09 | −34.08 |

[a] $Occ^M = (BP_{ND}\text{-baseline} - BP_{ND}\text{-pretreatment})/BP_{ND}\text{-baseline} \times 100\%$.